10. Y. Sato, T. Hirata, M. Ogawa, H. Fujisawa, *J. Neurosci.* **18**, 7800 (1998).
11. T. Hirata, H. Fujisawa, *J. Neurobiol.* **38**, 93 (1999).
12. A. Kawakami, T. Kitsukawa, S. Takagi, H. Fujisawa, *J. Neurobiol.* **29**, 1 (1996).
13. E. Steck *et al.*, *Biochem. J.* **353**, 169 (2001).
14. E. Steck *et al.*, *Matrix Biol.* **26**, 30 (2007).
15. J. C. Loftus, J. W. Smith, M. H. Ginsberg, *J. Biol. Chem.* **269**, 25235 (1994).
16. T. Hirokawa, S. Boon-Chieng, S. Mitaku, *Bioinformatics* **14**, 378 (1998).
17. A. E. Fournier, T. GrandPre, S. M. Strittmatter, *Nature* **409**, 341 (2001).
18. B. P. Liu, A. Fournier, T. GrandPré, S. M. Strittmatter, *Science* **297**, 1190 (2002); 10.1126/science1073031.
19. B. P. Liu, W. B. Cafferty, S. O. Budel, S. M. Strittmatter, *Philos. Trans. R. Soc. London Ser. B* **361**, 1593 (2006).
20. G. Yiu, Z. He, *Nat. Rev. Neurosci.* **7**, 617 (2006).
21. H. Tozaki, T. Kawasaki, Y. Takagi, T. Hirata, *Brain Res. Mol. Brain Res.* **104**, 111 (2002).
22. T. GrandPré, F. Nakamura, T. Vartanian, S. M. Strittmatter, *Nature* **403**, 439 (2000).

Acknowledgments: Supported by grants from the Core Research for Evolutionary Science Technology (CREST) of the Japan Science and Technology Agency (to Y.S., T.H., Y.G., and K.T.); grants-in-aid from the Ministry of Education, Culture, Sport, Science, and Technology of Japan (to T.H. and K.T.); grants from the Dr. Ralph and Marion Falk Medical Research Trust and the NIH (to S.M.S.); and a grant for Research and Development Project II (No. S2107) of Yokohama City University, Japan (to Y.G. and K.T.). The authors thank T. Takeyama and Y. Saito at the Olympus Corporation (Tokyo, Japan) for technical assistance with FALI; H. Sekiguchi-Kaneko, T. Okada, M. Ogawara, and S. Chen for technical assistance; and Y. Sasaki, K. Ogura, K. Nishiyama, H. Ito, and T. Takahashi for helpful discussions and comments. K.T. and Y.S. designed the study, and K.T. and Y.G. supervised the experiments, data analysis, and interpretation. The experiments were carried out by Y.S., M.I., Y.K., M.Y., N.Y., F.N., Y.A., and K.T. T.K. and T.H. generated the mouse cDNA expression library of the olfactory bulb and collaborated on the production of monoclonal antibodies. T.A. and H.K. collaborated on the generation of *crtac1B (lotus)*-deficient mice. S.M.S. collaborated on experiments using *ngr1*-deficient mice and NgR2-3. K.T. wrote the paper, and Y.S., F.N., N.Y., and Y.G. edited the manuscript. S.M.S. is a cofounder and consultant of Axerion Therapeutics. Yale University holds a patent licensed to Axerion Therapeutics related to Ngr1 receptor blockers for recovery from central nervous system damage. Yokohama City University has a patent pending on Crtac 1B(LOTUS) function in neuronal cell growth. Materials transfer agreements restrict the use of Crtac1B(LOTUS) knockout mice and NgR1 knockout mice and expression constructs of NgR1, NgR2, and NgR3 proteins.

Supporting Online Material

www.sciencemag.org/cgi/content/full/333/6043/769/DC1
Materials and Methods
Figs. S1 to S15
References (*23*–*33*)

10 February 2011; accepted 22 June 2011
10.1126/science.1204144

Integrating What and When Across the Primate Medial Temporal Lobe

Yuji Naya[1]* and Wendy A. Suzuki[1]

Episodic memory or memory for the detailed events in our lives is critically dependent on structures of the medial temporal lobe (MTL). A fundamental component of episodic memory is memory for the temporal order of items within an episode. To understand the contribution of individual MTL structures to temporal-order memory, we recorded single-unit activity and local field potential from three MTL areas (hippocampus and entorhinal and perirhinal cortex) and visual area TE as monkeys performed a temporal-order memory task. Hippocampus provided incremental timing signals from one item presentation to the next, whereas perirhinal cortex signaled the conjunction of items and their relative temporal order. Thus, perirhinal cortex appeared to integrate timing information from hippocampus with item information from visual sensory area TE.

Episodic memory, or the ability to mentally reexperience a previous event in one's life, is formed when individual events or items become bound to the specific temporal context in which the event took place (*1*, *2*). The human medial temporal lobe (MTL) is critical for episodic memory presumably because of its role in binding individual stimuli or events to their temporal and spatial contexts (*3*–*5*). Computation models (*6*, *7*) have proposed that cortical association areas signal information about items, parahippocampal regions signal information about items along with their temporal context, whereas hippocampus (HPC) supervises these item-context associations. Consistent with these model predictions, functional magnetic resonance imaging (fMRI) studies in humans report both HPC and parahippocampal activation during tasks of temporal-order memory (*8*, *9*). Recent neurophysiological studies in the rodent have highlighted the role of HPC in signaling either a particular time within a trial (*10*, *11*) or incremental timing across the entire recording session (*12*). However, little is known about the neurophysiological basis of how item and timing information is integrated within MTL. We therefore recorded neural activity from MTL areas and a control visual area (fig. S1) (*13*–*16*) as nonhuman primates performed a temporal-order memory task (*17*, *18*) that required encoding of two visual items and their temporal order (Fig. 1, A and B) (*19*).

A total of 644 neurons were recorded in the two macaques (table S1). We evaluated the effects of "time" and "item" on the cue responses separately for each neuron. We referred to neurons whose responses differentiated between the cue 1 and cue 2 periods on a two-tailed paired *t* test ($P < 0.01$) as "time cells" that could signal relative timing between cue presentations or temporal order of cue presentations. The neurons that showed significant stimulus-selective activity during either cue 1 or cue 2 on a one-way analysis of variance with the eight stimuli as a main factor ($P < 0.005$ for each cue) were referred to as "item cells." Numbers of these task-related neurons (time or item cells) were significantly greater than expected by chance (~2% of the recorded neurons) in all areas [53/193, HPC; 29/143, entorhinal cortex (ERC); 68/231, perirhinal cortex (PRC); 50/77 TE; $P < 0.0001$ for each area, χ^2 test]. We compared the proportions of time and item cells across areas and found the highest proportions of item cells in visual area TE, with gradually decreasing proportions seen in PRC, ERC, and HPC (Fig. 1C, open bars). In contrast, we observed the highest proportions of time cells in HPC (solid bars). The proportions of time cells and item cells were significantly different across areas ($P < 0.0001$, χ^2 test). These results suggest the possibility that

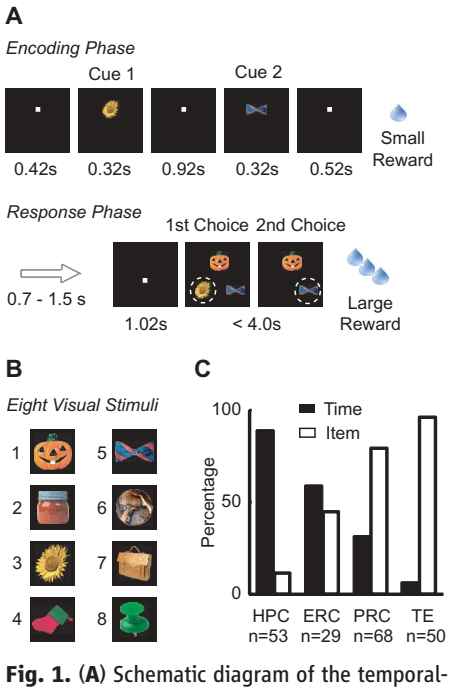

Fig. 1. (**A**) Schematic diagram of the temporal-order task. A sequence of two cue stimuli was presented in the encoding phase. The two cue items and one distracter were presented at three different positions randomly in the response phase. Dashed circles indicate correct targets. (**B**) The eight visual stimuli used in the task. (**C**) Relative proportions of time cells and item cells in each area.

[1]Center for Neural Science, New York University, 4 Washington Place, New York, NY 10003, USA.

*To whom correspondence should be addressed. E-mail: yujin@cns.nyu.edu

time information flows from HPC to ERC and PRC, whereas item information flows from TE to PRC and ERC.

We first examined the prominent time signals in HPC. Figure 2A shows an example of a typical time cell in HPC that showed stronger responses during cue 2 relative to cue 1. This cell started to respond in the middle of the delay period between cue 1 and cue 2 (i.e., cue 1 delay period) and continued firing strongly during cue 2. We also observed HPC time cells with high firing rates during cue 1 that decreased their activity substantially during the cue 1 delay period (Fig. 2B). This characteristic timing signal was also seen at the level of the local field potential (LFP). HPC started to increase its gamma band activity (>30 Hz) during the cue 1 delay period (Fig. 3A), and the gamma band activity in HPC was significantly stronger during cue 2 than cue 1 ($P < 0.0001$, two-tailed paired t test) (table S3). No such difference was observed in the other three areas (Fig. 3, B to D).

To characterize the temporal dynamics of time cells observed throughout the MTL, we applied a population vector analysis (*12*, *20*). We constructed n-dimensional vectors from the responses of time cells for 40-ms time bins throughout the cue 1 delay period, where "n" is the number of time cells in each area (*19*). In HPC, the distance of this vector from a "template" defined as the cue 1 state increased at a constant rate during the cue 1 delay period (Fig. 2C, solid circles) as evaluated by a polynomial curve fitting approach (table S4), whereas the distance to the cue 2 state (open squares) decreased at a constant rate. This pattern of activity was confirmed in both animals (fig. S3). These results indicated that, as a population, HPC time cells provide an incremental timing signal that gives an estimate of the relative time from the last cue presentation as well as an estimate of the relative time to the next cue presentation (fig. S7B). An incremental timing signal was not present in PRC, where there was a more sudden shift in the distance measures from both the cue 1 and cue 2 states early in the cue 1 delay period that then remained relatively constant for the remainder of the delay period (Fig. 2E). ERC appeared to exhibit an intermediate pattern such that the distance measures from the cue 1 state changed in a gradual manner but the distance to the cue 2 state did not (Fig. 2D). Principal component analysis of neuronal activity during the encoding phase also supported the idea of a strong incremental timing signal in HPC and a similar but weaker such signal in ERC (fig. S4). To determine which area provided the most accurate representation of the cue 2 state before the presentation of cue 2, we asked which of the three areas exhibited the shortest distance to the cue 2 state during the last quarter (240 ms) of the cue 1 delay period. We found that HPC exhibited the shortest distance to cue 2 (Fig. 2F).

We next examined the information carried by item cells in TE, PRC, and ERC. We first asked whether item cells represented the same

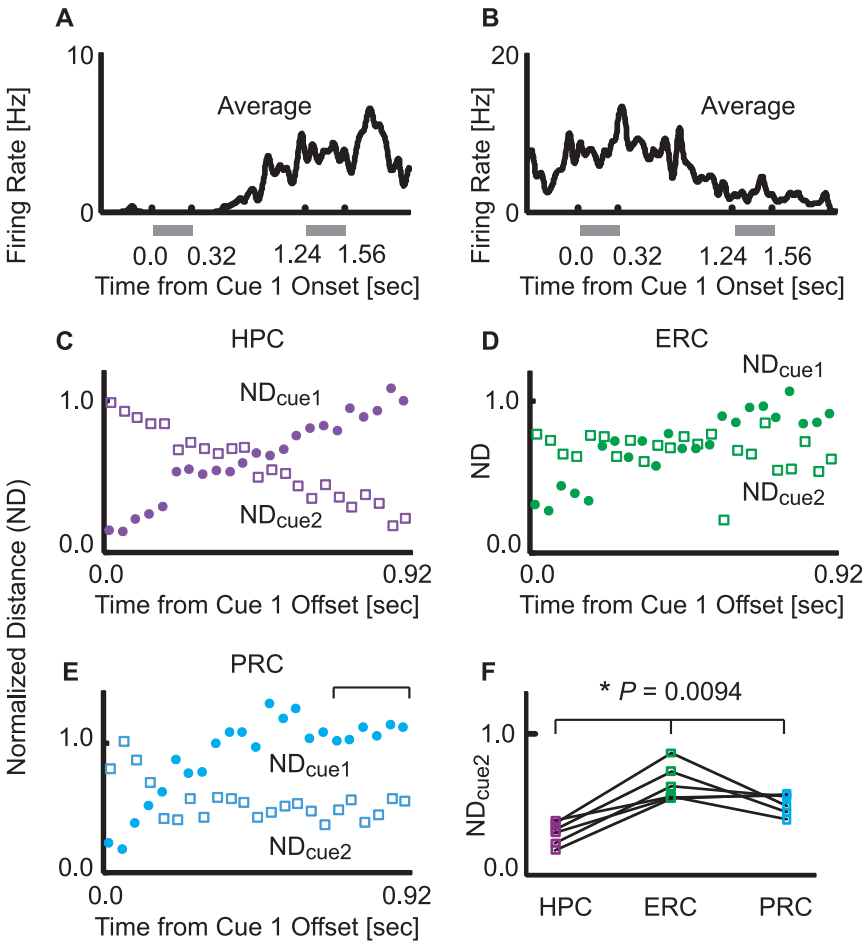

Fig. 2. (**A**) An example of an HPC time cell showing greater responses during cue 2 than cue 1. Shown is the average spike density function (SDF, σ = 20 ms) across all trials in the encoding phase. (**B**) An example of an HPC time cell showing greater responses during cue 1 than cue 2. (**C** to **E**) Normalized distances (NDs) from the cue 1 states (solid circles) and the cue 2 states (open squares) in each area. (**F**) Comparison of NDs to the cue 2 states during the last 240 ms (six bins) of the cue 1 delay period. The values at the same time points are connected by lines. The NDs were significantly different in the three areas (Friedman test).

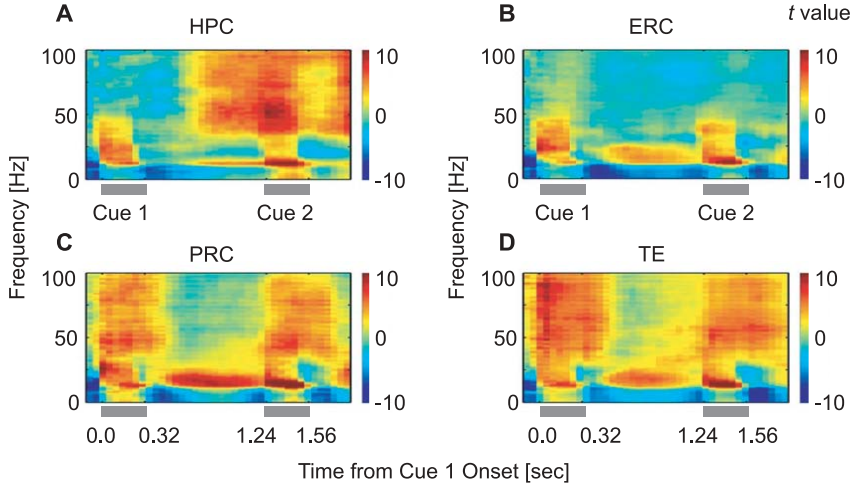

Fig. 3. (**A** to **D**) Two-dimensional plots of the population average LFP spectrogram in HPC ($n = 62$), ERC ($n = 54$), PRC ($n = 49$), and TE ($n = 29$). Time is on x axis; frequency is on y axis. Red pixels indicate time-frequency domains in which activity was stronger than that in control period (pixels centered on 150 ms and 100 ms before cue 1 onset). Blue pixels indicate the opposite pattern. The differential activities were evaluated by t values (paired t test).

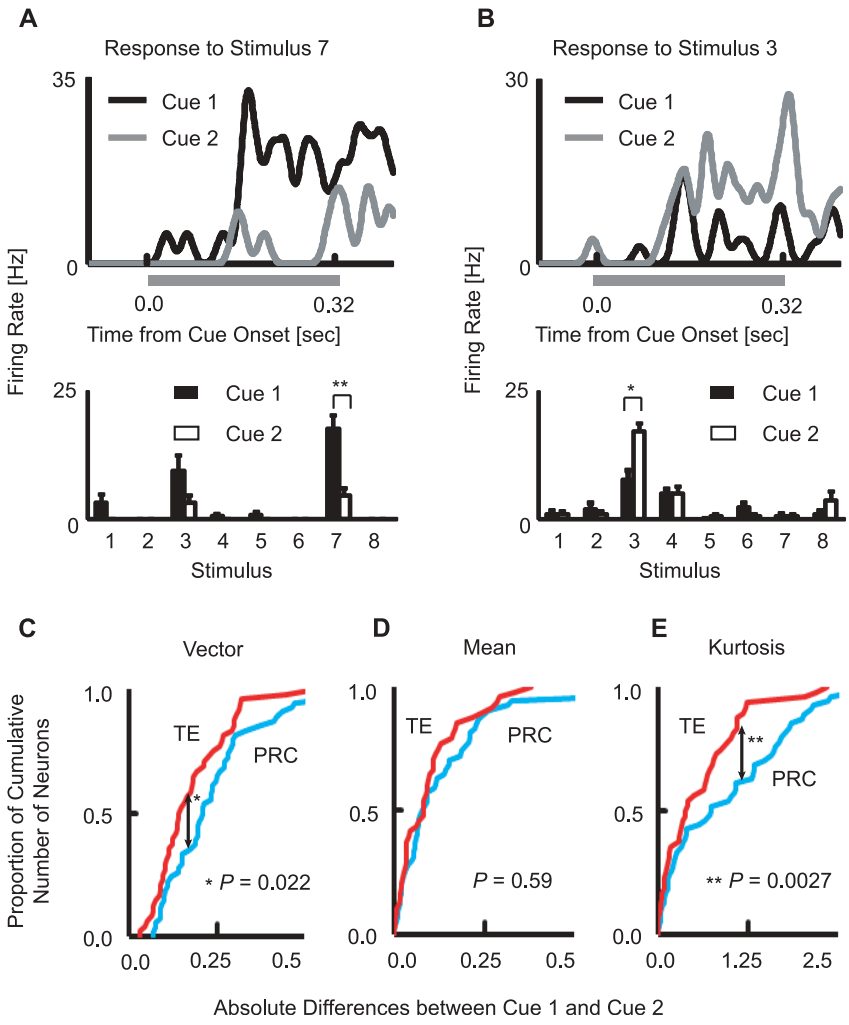

Fig. 4. (**A**) An example of a PRC item cell. (Top) SDFs to stimulus 7 for cue 1 superimposed with cue 2. (Bottom) Mean discharge rates and SEM during cue 1 and cue 2. Double asterisk, significantly different responses between cue 1 and cue 2 ($P = 0.002$, two-tailed t test). (**B**) Another example of a PRC item cell. (Top) SDFs to stimulus 3. (Bottom) The same formats as (A). Asterisk, $P = 0.012$. (**C**) Cumulative frequency histograms of normalized vector distances between cue 1 and cue 2 for PRC ($n = 54$; light blue) and TE ($n = 48$; red). (**D** and **E**) The same formats as (C) but for absolute differences of normalized mean discharge rates and kurtosis, respectively.

items across the two cue periods. To address this question, we analyzed the correlation coefficient between response amplitudes of all eight stimuli during cue 1 and cue 2 (*21*). The correlation coefficients in ERC (median = 0.62) were significantly smaller than either PRC (median = 0.86; $P = 0.0077$, Kolmogorov-Smirnov test) or TE (median = 0.90; $P = 0.0017$). The small correlation coefficients in ERC can be explained by the lack of stimulus selectivity in one of the two cue periods (fig. S5). This differential level of stimulus selectivity between cue periods can serve to integrate item information with a relative timing signal [supporting online material (SOM) text]. In contrast, PRC and TE represented the same items across the two cue periods. Closer examination of these responses revealed a time effect in PRC such that the response to the neuron's preferred stimulus differed across cue 1 and cue 2 (Fig. 4, A and B). This temporal modulation for preferred items was observed for the entire population of PRC item cells (fig. S6A), suggesting that these cells may integrate item and temporal order information by modulating their stimulus-selective response properties across the cue periods.

To test this hypothesis, we defined two vectors consisting of the response amplitudes to the eight stimuli presented during cue 1 or cue 2. The distance between the two vectors was normalized by the sum of the two vectors' lengths. The normalized distances were significantly greater for item cells in PRC compared with those in TE (Fig. 4C, $P = 0.022$, Kolmogorov-Smirnov test), suggesting a more prominent time effect in PRC. This differential time effect between PRC and TE could be explained either by general increases or decreases in firing rates or by changes in tuning curve sharpness across the two cue periods. When we compared the mean responses to all eight stimuli between the two cue periods, we found no differential time effect between the two areas (Fig. 4D, $P = 0.59$). By contrast, when we examined the sharpness of the tuning curve during the two cue periods using a kurtosis measure (*21*, *22*), we found the absolute difference of the measures between the two cue periods was significantly greater in PRC compared with TE (Fig. 4E, $P = 0.0027$). This suggests that PRC differentiates between the cue 1 and cue 2 periods by changing the sharpness of its stimulus-selective response.

The present study provides insight about how individual MTL structures may integrate item and timing information (i.e., "what" and "when") in the service of episodic memory (*6*–*9*) (fig. S7). HPC provides a robust incremental timing signal (*10*–*12*) that may serve to anchor the timing to events within an episode (*23*). Consistent with predictions from previous computational models (*6*, *7*), our data show that PRC neurons integrate time and item information by modulating their stimulus-selective response properties across temporally distinct stimulus presentations. ERC neurons can signal incremental timing information as well as integrate item and time information, albeit at a lower magnitude than HPC or PRC, respectively. We hypothesize that the incremental timing signal in HPC is conveyed to PRC via ERC, where it is integrated with item information from TE and converted into a discrete item-based temporal order signal.

References and Notes

1. H. Eichenbaum, N. Fortin, *Curr. Dir. Psychol. Sci.* **12**, 53 (2003).
2. E. Tulving, *Annu. Rev. Psychol.* **53**, 1 (2002).
3. J. J. Downes, A. R. Mayes, C. MacDonald, N. M. Hunkin, *Neuropsychologia* **40**, 853 (2002).
4. F. Vargha-Khadem *et al.*, *Science* **277**, 376 (1997).
5. M. Moscovitch, L. Nadel, G. Winocur, A. Gilboa, R. S. Rosenbaum, *Curr. Opin. Neurobiol.* **16**, 179 (2006).
6. M. W. Howard, M. J. Kahana, *J. Math. Psychol.* **46**, 269 (2002).
7. M. W. Howard, M. S. Fotedar, A. V. Datey, M. E. Hasselmo, *Psychol. Rev.* **112**, 75 (2005).
8. L. J. Jenkins, C. Ranganath, *J. Neurosci.* **30**, 15558 (2010).
9. S. Tubridy, L. Davachi, *Cereb. Cortex* **21**, 272 (2011).
10. E. Pastalkova, V. Itskov, A. Amarasingham, G. Buzsáki, *Science* **321**, 1322 (2008).
11. P. R. Gill, S. J. Mizumori, D. M. Smith, *Hippocampus* 10.1002/hipo.20832 (2010).
12. J. R. Manns, M. W. Howard, H. Eichenbaum, *Neuron* **56**, 530 (2007).
13. W. A. Suzuki, D. G. Amaral, *J. Comp. Neurol.* **350**, 497 (1994).
14. Y. Naya, M. Yoshida, Y. Miyashita, *Science* **291**, 661 (2001).
15. S. Wirth *et al.*, *Science* **300**, 1578 (2003).
16. K. Tanaka, *Annu. Rev. Neurosci.* **19**, 109 (1996).
17. Y. Ninokura, H. Mushiake, J. Tanji, *J. Neurophysiol.* **89**, 2868 (2003).
18. M. R. Warden, E. K. Miller, *Cereb. Cortex* **17** (suppl. 1), i41 (2007).
19. Information on materials and methods are available on *Science* Online.
20. O. Barak, M. Tsodyks, R. Romo, *J. Neurosci.* **30**, 9424 (2010).
21. Y. Naya, M. Yoshida, Y. Miyashita, *J. Neurosci.* **23**, 2861 (2003).
22. S. R. Lehky, T. J. Sejnowski, R. Desimone, *Vision Res.* **45**, 57 (2005).
23. R. Paz *et al.*, *Proc. Natl. Acad. Sci. U.S.A.* **107**, 6046 (2010).

Acknowledgments: The present study was funded by NIH grants RO1 MH086563 to W.A.S. and Y.N. and RO1 MH058847 to W.A.S. We thank E. Wang, A. Shang, and N. Nystrom for expert animal care and E. Hargreaves, M. Yanike, and M. Shapiro for helpful comments. The authors declare no competing financial interests. Y.N. and W.A.S. designed the experiments and wrote the manuscript. Y.N. performed the experiment and analyzed the data.

Supporting Online Material
www.sciencemag.org/cgi/content/full/333/6043/773/DC1
Materials and Methods
SOM Text
Figs. S1 to S7
Tables S1 to S5
References (*24*–*35*)

11 April 2011; accepted 21 June 2011
10.1126/science.1206773

Google Effects on Memory: Cognitive Consequences of Having Information at Our Fingertips

Betsy Sparrow,[1]* Jenny Liu,[2] Daniel M. Wegner[3]

The advent of the Internet, with sophisticated algorithmic search engines, has made accessing information as easy as lifting a finger. No longer do we have to make costly efforts to find the things we want. We can "Google" the old classmate, find articles online, or look up the actor who was on the tip of our tongue. The results of four studies suggest that when faced with difficult questions, people are primed to think about computers and that when people expect to have future access to information, they have lower rates of recall of the information itself and enhanced recall instead for where to access it. The Internet has become a primary form of external or transactive memory, where information is stored collectively outside ourselves.

In a development that would have seemed extraordinary just over a decade ago, many of us have constant access to information. If we need to find out the score of a ball game, learn how to perform a complicated statistical test, or simply remember the name of the actress in the classic movie we are viewing, we need only turn to our laptops, tablets, or smartphones and we can find the answers immediately. It has become so commonplace to look up the answer to any question the moment it occurs that it can feel like going through withdrawal when we can't find out something immediately. We are seldom offline unless by choice, and it is hard to remember how we found information before the Internet became a ubiquitous presence in our lives. The Internet, with its search engines such as Google and databases such as IMDB and the information stored there, has become an external memory source that we can access at any time.

Storing information externally is nothing particularly novel, even before the advent of computers. In any long-term relationship, a team work environment, or other ongoing group, people typically develop a group or transactive memory (*1*), a combination of memory stores held directly by individuals and the memory stores they can access because they know someone who knows that information. Like linked computers that can address each other's memories, people in dyads or groups form transactive memory systems (*2*, *3*). The present research explores whether having online access to search engines, databases, and the like, has become a primary transactive memory source in itself. We investigate whether the Internet has become an external memory system that is primed by the need to acquire information. If asked the question whether there are any countries with only one color in their flag, for example, do we think about flags or immediately think to go online to find out? Our research then tested whether, once information has been accessed, our internal encoding is increased for where the information is to be found rather than for the information itself.

In experiment 1, participants were tested in two within-subject conditions (*4*). Participants answered either easy or hard yes/no trivia questions in two blocks. Each block was followed by a modified Stroop task (a color-naming task with words presented in either blue or red) to test reaction times to matched computer and noncomputer terms (including general and brand names for both word groups). People who have been disposed to think about a certain topic typically show slowed reaction times (RTs) for naming the color of the word when the word itself is of interest and is more accessible, because the word captures attention and interferes with the fastest possible color naming.

Paired within-subject t tests were conducted on color-naming reaction times to computer and general words after the easy and difficult question blocks. Confirming our hypothesis, computer words were more accessible [color-naming RT mean (M) = 712 ms, SD = 413 ms] than general words (M = 591 ms, SD = 204 ms) after participants had encountered a series of questions to which they did not know the answers, $t(68) = 3.26$, $P < 0.003$, two-tailed. It seems that when we are faced with a gap in our knowledge, we are primed to turn to the computer to rectify the situation. Computer terms also interfered somewhat more with color naming (M = 603 ms, SD = 193 ms) than general terms (M = 559 ms, SD = 182 ms) after easy questions, t (68) = 2.98, $P < 0.005$, suggesting that the computer may be primed when the concept of knowledge in general is activated.

Comparison using a repeated measures analysis of variance (ANOVA) of specific search engines (Google/Yahoo) and general consumer-good brand names (Target/Nike) revealed an interaction with easy versus hard question blocks, $F(1,66) = 5.02$, $P < 0.03$, such that search engine brands after both easy questions (M = 638 ms, SD = 260 ms) and hard questions (M = 818 ms, SD = 517 ms) created more interference than general brands after easy questions (M = 584 ms, SD = 220 ms) and hard questions (M = 614 ms, SD = 226 ms) (Fig. 1). Simple effects tests showed that the interaction was driven by a significant increase in RT for the two search engine terms after the hard question block, $F(1,66) = 4.44$, $P < 0.04$ (Fig. 1). Although the concept of knowledge in general seems to prime thoughts of computers, even when answers are known, not knowing the answer to general-knowledge questions primes the need to search for the answer, and subsequently computer interference is particularly acute.

In experiment 2, we tested whether people remembered information that they expected to have later access to—as they might with information they could look up online (*4*). Participants were tested in a 2 by 2 between-subject experiment by reading 40 memorable trivia statements of the type that one would look up online (both of the new information variety, e.g., "An ostrich's eye is bigger than its brain," and information that may be remembered generally, but not in specific detail, e.g., "The space shuttle Columbia disintegrated during re-entry over Texas in Feb. 2003."). They then typed them into the computer to ensure attention (and also to provide a more generous test of memory). Half the participants believed the computer would save what was typed; half believed the item would be erased. In addition, half of the participants in each of the saved and erased conditions were asked explicitly to try to remember the information. After the reading and typing task, participants wrote down as many of the statements as they could remember.

[1]Department of Psychology, Columbia University, 1190 Amsterdam Avenue, New York, NY 10027, USA. [2]Department of Psychology, University of Wisconsin–Madison, 1202 West Johnson Street, Madison, WI 53706, USA. [3]Department of Psychology, Harvard University, 33 Kirkland Street, Cambridge, MA 02138, USA.

*To whom correspondence should be addressed. E-mail: sparrow@psych.columbia.edu

www.sciencemag.org/cgi/content/full/333/6043/773/DC1

Supporting Online Material for

Integrating What and When Across the Primate Medial Temporal Lobe

Yuji Naya* and Wendy A. Suzuki

*To whom correspondence should be addressed. E-mail: yujin@cns.nyu.edu

Published 5 August 2011, *Science* **333**, 773 (2011)
DOI: 10.1126/science.1206773

This PDF file includes:

Supporting Online Material

1. Materials and methods

Subjects: Two male rhesus monkeys (8.1 kg, monkey B; 10.3 kg, monkey G) were used for the experiments. All procedures and treatments were done in accordance with NIH guidelines and approved by the New York University Animal Welfare Committee.

Behavioral task: We trained the two animals on a temporal-order task with visual objects (Fig. 1A). The task started with an encoding phase which was initiated by the animal fixating on a fixation point on a video monitor for 0.42 s. Eye position was monitored by infrared digital camera. Then, a sequence of two cue stimuli was presented for 0.32 sec each with a 0.92 sec delay interval between them (cue 1 delay period). The additional 0.02 s added to each trial event derived from the design of software controlling the behavioral task. Cue stimuli were pseudo-randomly chosen out of a pool of eight well-learned visual items (Fig. 1B), resulting in 56 (8X7) different 2-stimulus sequences. The same eight stimuli were used during all recording sessions. Following the second cue stimulus, another 0.52 s delay interval requiring fixation was shown. If fixation was successfully maintained, the encoding phase ended with the presentation of a single drop of water. The encoding phase was followed by a blank inter-phase delay interval of 0.7-1.5 s where no fixation was required. The response phase started with a pre-response delay period of 1.02 s with fixation required. Then, three choice stimuli were presented simultaneously on the screen: two of them were the items that had been presented as cue stimuli in the encoding phase, and the third was a distracter stimulus chosen from the pool of the remaining 6 possible items. If the animal touched the two cue items in the same temporal order as they were presented in the encoding phase, six or seven drops of

water were given as a reward. Following behavioral training, the two monkeys performed the task at 87.9 ± 5.3 % (mean ± standard deviation; monkey B, n = 359 sessions) and 88.1 ± 5.0 % (monkey G, n = 199 sessions) for the 1st cue choice, and 83.1 ± 12.3 % (monkey B) and 77.8 ± 8.6 % (monkey G) for the 2nd cue choice.

Electrophysiological recording: Following initial behavioral training, the animals were implanted with a head post and recording chamber under aseptic conditions using isoflurane anesthesia. To record single-unit activity, we used individual tungsten tetrodes or single-wire tungsten microelectrodes advanced into the brain with a hydraulic microdrive. The microelectrodes were inserted through a stainless steel guide tube positioned in a grid system on the recording chamber. Neural signals for single-units were collected (low-pass, 8 kHz; high-pass, 250 Hz) and digitized (40 kHz). These signals were sorted by an off-line sorter. We made no attempt to prescreen isolated neurons. Instead, once we succeeded in isolating any neuron, we started a new recording session. To record LFPs, we used neural signals from the same tetrodes or single-wire electrodes as we used for the recording of spikes. However, the signals were collected using different filters (low-pass, 170 Hz; high-pass 0.7 Hz), and digitized at 1 kHz. Here, we focused on the LFP data gathered with a pre-amplifier gain setting of X1000 which provided a favorable signal to noise ratio.

Placement of microelectrodes into the target areas was guided by the individual brain atlases from MRI scans (3T). We also constructed individual brain atlases from the electrophysiological properties around the tip of the electrode (e.g. gray matter, white matter, sulcus, lateral ventricle, and bottom of the brain). The recording sites were estimated by combining the individual MRI atlases and the physiological atlases. After

the recording sessions, we confirmed recording sites in the right hemisphere of Monkey G by MR images identifying the position of a single tungsten electrode placed in a central recording position. The recording sites in the right hemisphere of Monkey B were confirmed by MRI-detectable metal deposits (fig. S1) (*24*, *25*) made by passing anodic current of 5μA for 5 min from a tip of a single-wire stainless steel microelectrode. We made a total of 15 deposits along 7 penetrations of the microelectrodes. The metal deposit marks appeared as hypointense spots on MR images using a FLASH sequence.

The recording sites covered between 14 and 23 mm anterior to the interaural line (fig. S1). The recording sites in HPC appeared to cover all of its subdivisions (i.e., dentate gyrus, CA3, CA1, and subicular complex). The recording sites of ERC focused on approximately lateral 2/3 of the anterior portion of ERC. The recording sites in PRC appeared to cover both area 35 and 36 from the fundus of rhinal sulcus to medial lip of anterior middle temporal sulcus (amts). The recording sites in TE were limited to anterior ventral area of TE including both banks of amts. A final determination will require histological verification (both animals are currently still being used).

Data analysis for all recorded neurons: All neuronal data were analyzed with custom-written Matlab programs including the statistics toolbox. We defined a cue response as the firing rate during the period extending from 80 to 400 msec after the cue onset; we used an 80 msec shift to compensate for the latency of visual response. We evaluated the effects of 'time' and 'item' separately for each neuron. To examine the effect of item, we tested differential stimulus selectivity for cue 1 and cue 2 separately using a one-way ANOVA with the 8 stimuli as a main factor. We analyzed the time and item effects separately to better characterize the heterogeneous nature of the signals seen across the 4

brain areas (HPC, ERC, PRC and TE). To correct for the effect of multiple comparisons on the item effects, we set the significance level to $P < 0.005$ for each cue period. This matched the significance level we used to identify time effects ($P < 0.01$). While we did not find a clear laterality effect in the proportions of item and time cells across the areas (table S2), the majority of the neurons were recorded in the right hemispheres in both monkeys (84% for monkey B, 62% for monkey G), precluding a strong conclusion. Our time cell analyses focused on HPC, ERC and PRC (too few time cells in TE) and our analyses of item cells focused on TE, PRC and EC (too few item cells in HPC). Neural activity in the response phase will be described in a separate publication.

Data analysis for time cells: We constructed a population vector from the responses of all individual time cells in each area and characterized their temporal dynamics during the cue 1 delay period relative to two "template" time periods defined as the cue 1 and the cue 2 presentation periods. Previous studies used a direct calculation of the distance between population vectors during equivalent time periods in two separate trials (*12*). However, the present study handled qualitatively distinct time periods within single trials: two cue presentations ("templates") and a delay period between them ("target"). In this situation, distance measures are influenced by 1) the ratio of activity between the "template periods" and the "target period" and 2) the difference in the level of activity between the "template periods". To evaluate these two factors independently, we first compared the population vector activity during the cue 1 delay period with 1) the sum of the activity during the two cue periods and 2) the difference of the activity between the two cue periods.

We calculated mean firing rates of consecutive 40 ms time bins across all completed trials from cue 1 onset to cue 2 offset (39 bins) for each neuron. Using the 39 bins, we calculated a set of z-scores and assigned a point to each time bin in n-dimensional space for each area, where 'n' was the number of time cells in the corresponding area. The n-dimensional vector at each time-bin was then projected onto a two-dimensional space constructed by two unit-vectors:

1) "sum", $Xs = (R_{cue1} + R_{cue2})/| R_{cue1} + R_{cue2}|$

2) "difference", $Xd = (R_{cue2} - R_{cue1})/| R_{cue1} - R_{cue2}|$

Where R_{cue1} and R_{cue2} are n-dimensional vectors consisting of average z-values during the 120-320 ms after the onset of cue 1 and cue 2, respectively. The positions on the two-dimensional space were represented by β coefficient estimates for a generalized linear regression (*26*):

$$Y(t) = \beta_0(t) + \beta s(t)*Xs + \beta d(t)*Xd$$

Xs and Xd act as predictors. Y(*t*) is a set of z-values at time '*t*' and are dependent variables. βs(*t*) and βd(*t*) were calculated as coefficient estimates for the predictors of "sum" and "difference" at each time '*t*', respectively. $\beta_0(t)$ is a coefficient estimate for a constant term.

After evaluating the effects of "sum" and "difference" on the population vector activity during the cue 1 delay period (fig. S2 and supporting text 2.1), we combined these two measures to estimate the distances from the cue 1 or cue 2 states (Fig. 2, C-F). The distances from the cue 1 or cue 2 states were defined by the equations: '| (βs(*t*) - βs1)*Xc + (βd(*t*) – βd1)*Xd |' or '| (βs(t) - βs2)*Xc + (βd(t) – βd2)*Xd |', respectively.

These distances were normalized by the distance between the two cue states, '| (βs2 - βs1)*Xc + (βd2 – βd1)*Xd |' (Fig. 2, C-F). Note that the present results were consistent with those from a direct calculation of distance between each template and the population vectors during the cue 1 delay period.

Data analysis for item cells: To evaluate the time effect for each item cell, we first prepared two vectors: $FR_{c1} = (fr_{11} — fr_{18})$ and $FR_{c2} = (fr_{21} — fr_{18})$, where fr_{ij} denotes the mean cue response for the *j*-th stimulus during the *i*-th cue period. The correlation coefficient between FR_{c1} and FR_{c2} was defined as $r = \Sigma[(fr_{1j} – \mu_1)(fr_{2j} – \mu_2)]/\{ [\Sigma (fr_{1j} – \mu_1)^2)][\Sigma (fr_{2j} – \mu_2)^2)]\}^{1/2}$ (j = 1 — 8). μ_1 and μ_2 are the averages of fr_{1j} and fr_{2j}. The distance between FR_{c1} and FR_{c2} was calculated as $d = [\Sigma (fr_{1j} – fr_{2j})^2]^{1/2}$ (j = 1 — 8) for each neuron. It was normalized as $d' = d/\{[\Sigma (fr_{1j})^2]^{1/2} + [\Sigma (fr_{2j})^2]^{1/2}\}$ (j = 1 — 8). Kurtosis was defined for each of FR_{c1} and FR_{c2} as $k_i = E[(fr_{ij}– \mu_i)^4]/\sigma_i^4$ (i = 1 or 2, j = 1 — 8) where σ_i is the SD of fr_{ij} and E(X) is the expected value of X. The kurtosis of the normal distribution is 3. Greater value of the kurtosis indicates greater effect of outliers. The absolute difference of normalized mean discharge rates between the two cues was defined as $| \mu_1 – \mu_2 | / (\mu_1 + \mu_2)$.

Data analysis for local field potential: For the spectral analysis of the LFPs, we used the CHRONUX toolbox developed by P. Mitra at Cold Spring Harbor Laboratories (*27*, *28*). Multi-tapering method is useful for spectral estimation on finite time segments because it can maximize spectral concentration in a given frequency band by using an appropriate set of orthogonal tapers. We used the discrete prolate spheroidal sequences or Slepian sequences, which are defined by the property that they are maximally localized in the frequency band. In the multitaper method, we first calculated spectra

estimates for individual tapers as Fourier transforms of the data multiplied by them. We next averaged the tapered Fourier transforms. Using five Slepian tapers, we estimated LFP spectrum on a 300 ms window with 10 Hz resolution. The time windows were stepped at 50 ms intervals.

We examined LFP activity during cue 1 and cue 2 in the beta band, in the low frequency gamma band and in the high frequency gamma band. We first calculated mean values of log-scaled powers for each recording site, from pixels centered on 15 Hz to 25 Hz for the beta band, from 35 Hz to 50 Hz for low-frequency gamma band and from 70 Hz to 90 Hz for high-frequency gamma band. We then averaged the values along the time axis during the period centered on 0 ms to 300 ms after the cue onset. These values were compared with the mean values during the control period centered on 150 ms and 100 ms before the cue 1 onset in the corresponding frequency band (table S3). If there was a significant change of activity from the control period to cue 1 or cue 2 ($P < 0.05$, two-tailed paired t-test), we then compared the activity between cue 1 and cue 2 (two-tailed paired t-test). Note that the differential gamma band activities of HPC across the two cue periods cannot be explained by the activity of single-units because the average responses for the time cells in HPC were not different ($P = 0.11$, two-tailed paired t-test) between cue 1 (mean ± s.e.m. = 7.0 ± 0.8 Hz) and cue 2 (8.5 ± 1.1 Hz). We also note that HPC gamma-band activity showed a trough after cue 2 offset (Fig. 3A), suggesting that the increased activity during cue 1 delay was not consistent with the reward expectancy.

2. Supporting text

2.1 Population vector analysis: The results of our regression analysis (see materials and methods) showed that β coefficients for the predictor "sum" [βs(*t*)] showed negative values during the cue 1 delay period in HPC, ERC and PRC (fig. S2, left column, open squares) and the values were more close to zero in HPC (median = -0.21 during the last 600 ms) compared with the other two areas (-0.40 for ERC and -0.37 for PRC), indicative of the differential visual response effects across the areas. We also found differences in the time courses of β coefficients for the predictor "difference" [βd(*t*)] across the areas (fig. S2, left column, filled circles). In HPC, βd(*t*) exhibited a prominent gradual increase from negative to positive values during the cue 1 delay period (fig. S2A). The βd(*t*) values in ERC also showed a gradual increase after the cue 1 offset, though the slope of the increase appeared less steep than in HPC (fig. S2C). In PRC, after a sudden shift following cue 1 offset, the βd(*t*) values did not show a clear increase during the remainder of the cue 1 delay period (fig. S2E).

We plotted the two coefficients on a 2-dimensional scatterplots (fig. S2, right column). The states of cue 1 and cue 2 on the two-dimensional space were defined as the averages of βs(*t*) and βd(*t*) during 120-320 ms after the onset of cue 1 (βs1, βd1) and cue 2 (βs2, βd2). The HPC showed a trajectory of the population-state that was straight and gradually progressed from cue 1 to cue 2 on the two-dimensional space (fig. S2B). In contrast, the population states seen in ERC and PRC moved away from the cue 1 state quickly after cue 1 offset, and remained far from the cue 2 state during the cue 1 delay period (figs. S2, D and F).

2.2 Evaluating the temporal dynamics of the normalized distance measures: The temporal dynamics of the normalized distances from cue 1 (ND_{cue1}) and cue 2 (ND_{cue2}), and their sum ($ND_{cue1} + ND_{cue2}$) during the cue 1 delay period were evaluated by 0th, 1st and 2nd polynomial curves (table S4). Norms of the residuals to the polynomial fitting curves for ND_{cue1} and ND_{cue2} in HPC were greatly reduced from the 0th order to 1st order ($1.3 \rightarrow 0.28$ for ND_{cue1}, $1.1 \rightarrow 0.23$ for ND_{cue2}, $P < 0.0001$ for both, f-test). The fits to the 1st order of polynomial curves were good ($R^2 = 0.95$ for ND_{cue1}, 0.96 for ND_{cue2}) and the fits were not improved by the 2nd order polynomial curves ($P = 0.39$ for ND_{cue1}, 0.50 for ND_{cue2}). These results indicated that ND_{cue1} and ND_{cue2} changed at constant rates in HPC. The norm of the residuals to the 0th order of polynomial fitting curves for the sum of ND_{cue1} and ND_{cue2} was small (0.28), and was not significantly improved by the higher order polynomial curves. This result indicated that the sum of the distances from the cue 1 states and the cue 2 states did not change during the cue 1 delay period. In contrast to HPC, ND_{cue1} and ND_{cue2} in PRC were not well fitted by the 1st order of polynomial curve ($R^2 = 0.64$ for ND_{cue1}, 0.30 for ND_{cue2}). In ERC, the fit of ND_{cue1} was significantly ($P = 0.0006$) improved by the 1st order of polynomial curve ($R^2 = 0.78$) compared with the 0th order of polynomial curves ($R^2 = 0.10$), but not for ND_{cue2} ($P = 0.45$).

2.3 Principal component analysis: We examined the temporal features of time cells in each area using a principal component analysis (*29*). The population-vector analysis shown in Figures 2, C to F, S2 and S3 characterized a population state during the cue 1 delay period by relating it to the cue 1 and cue 2 states. By contrast, the principal component analysis simply extracts common features of the temporal dynamics across a neuronal population. Similar to the population vector analysis, we first calculated mean

firing rates of consecutive 40 ms time bins across all completed trials for each time cell. Using the firing rates from 320 ms before cue 1 onset to 400 ms after cue 2 offset (57 bins), we calculated a set of z-scores for each neuron. Using 'n' sets of z-scores, we conducted a principal component analysis and got the first and second principal component scores for each time bin, where 'n' is a number of time cells in each area. We also got proportions of corresponding principal components in each area and their coefficients for each time cell. In HPC, scores of the first principal component (proportion = 50.5%) changed gradually during the cue 1 delay period (fig. S4). The scores during the cue 1 delay period were well fitted ($R^2 = 0.99$) by a 1st order polynomial curve. This result is consistent with the results of the population-vector analysis (Fig. 2C). The scores remained relatively constant after cue 2 including the cue 2 delay period ($P = 0.50$, 0th vs. 1st order of polynomial curve fittings), suggesting that the incremental HPC timing signal during the cue 1 delay period is not related with reward expectancy. The distribution of the coefficients showed that the time cells in HPC were separable into two groups, one with positive signs (n = 29) and the other with negative signs (n = 19). These tendencies were also observed for time cells in ERC. The scores of the first component in ERC during the cue 1 delay period were well fitted by a 1st order polynomial curve ($R^2 = 0.86$) although its proportion of the first component (35.6%) was smaller than that of HPC. These findings suggest that while the ERC provides some incremental timing information, this signal is less prominent than that seen in HPC.

In PRC, we conducted the principal component analysis for time only cells (n = 14) and time & item cells (n = 7) separately. In both cases, the scores of the first components changed rapidly after the cue 1 offset but remained at relatively constant

values until the cue 2 presentation. The scores during the cue 1 delay period were well fitted by the 2nd order polynomial curves (R^2 = 0.87 for both) but not by the first order curves (R^2 = 0.54 for time only, R^2 = 0.50 for time & item). These results are consistent with the results from the population vector analysis (Fig. 2E) and indicate that both the PRC time only cells and the PRC time & item cells are distinct from HPC and ERC time cells. Note that we found no time & item cell in HPC and only one time & item cell in ERC (table S1).

2.4 Correlation analysis: When we examined the correlation coefficients between the response amplitudes to the 8 stimuli during cue 1 and cue 2 for item cells in TE, PRC and ERC, an effect of two different categories of item cells emerged. Type 1 item cells showed stimulus selectivity during both cue 1 and cue 2 periods while Type 2 item cells showed stimulus selectivity during only one of the two cue periods. For all areas examined, the magnitude of the correlation coefficient was higher for Type 1 compared to Type 2 item cells (fig. S5). However, ERC was unique in that it exhibited a much larger proportion of Type 2 item cells (69%) relative to Type 1 item cells (31%) compared to either PRC or TE (fig S5). These ERC Type 2 item cells provide a relative timing signal by showing stimulus-selectivity in only one of the two cue periods. Thus, ERC can signal item and temporal order information by modulating its stimulus selective responses across the two cue periods. Note that this seems to be a variation of the same stimulus-selective response modulation that integrates item and temporal order information observed in PRC (See main text and Fig. 4).

2.5 Further examination of the time effects of PRC item cells: Examples of PRC item cells shown in figures 4, A and B exhibited a striking time effect such that the

response to the neuron's preferred stimulus differed between cue 1 and cue 2. We asked if this pattern was seen for the entire population of the item cells in PRC. We calculated a mean of cue 1 and cue 2 responses to each item for each neuron. The 8 items were ranked from best (highest firing rate) to worst (lowest firing rate) and the responses during cue 1 and cue 2 were compared using a two-tailed t-test ($P < 0.05$). These time effects were most often observed for the best items (26%; fig. S6A). We also found significant numbers of neurons that showed the time effects to the second-ranked items (20.3%, $P = 0.034$). In contrast to the best and second best items, the frequencies of item cells with significant time effects were not different from the chance level for the remaining 6 items. These results indicate that the time effect in PRC item cells is specific for preferred items.

We compared the number of PRC item cells that showed stronger responses during cue 1 relative to cue 2 with cells that showed stronger responses during cue 2 relative to cue 1 (fig. S6B). The number of cue 1-preferring neurons (n = 23) did not differ from the number of cue 2-preferring neurons (n = 31) ($P = 0.44$, chi-square test), suggesting that this time effect cannot be explained by a simple attention effect to either of the cues. Next, we examined the time-course for the time effect in PRC item cells. Figures S6, C and D show the time course of responses to the best items for the total population of PRC item cells (n = 54) and for the item cells showing significant time effect (n = 14). In contrast to the incremental timing signal in HPC which spanned the entire cue 1 delay period (Fig. S7B), PRC item cells showed the time effect only associated with the cue presentation (fig. S7D).

2.6 Time and item representation in MTL: HPC provides an incremental timing signal during the cue 1 delay period between two item presentations and distinguishes the state of first item presentation from the second one regardless of item identity (fig. S7B). This suggests that HPC represents time between the two cue events in a continuous manner. PRC doesn't provide such an incremental timing signal during the cue 1 delay period (fig. S7D). Instead, PRC provides a strong representation of item identity during the cue periods and this strong item-based response is modulated as a function of temporal order (i.e., first, versus second; fig. S7D). Like HPC and PRC, ERC exhibits both an incremental timing signal as well as provides temporally modulated item signals. However, the magnitudes of both these signals are weaker than those seen in HPC or PRC (fig. S7C). We hypothesize that item information from TE and incremental timing signals from HPC via ERC converge on PRC where item and time information are integrated. In addition, weak direct projections from HPC directly to PRC (*30*) may also participate in this integrative information processing.

2.7 Spatial distributions of task-related neurons within each MTL area: While we are not able to specify the exact hippocampal recording locations with histology because both animals are still being used for experiments, we examined the gross topographic locations and relative proportions of the time cells along the dorsal-ventral and anterior-posterior axes of HPC from the MRI-based recording locations (fig. S1). To address this question, we first divided the HPC region on each coronal MRI section into a dorsal subdivision mainly including area CA3 and a ventral subdivision including mainly area CA1 and the subicular complex and next divided our HPC recording site into 3 anterior-posterior subdivisions. We didn't find a significant difference in proportions of the time

cells across the six subdivisions (table S5; $P = 0.40$, chi-square test), indicating that the time signal is represented by several subregions within HPC. Moreover, proportions of the time cells did not differ along either the dorsal-ventral axis ($P = 0.42$) nor the anterior-posterior axis ($P = 0.92$). These findings suggest that neurons throughout HPC subdivisions including both CA3 and CA1 participate in coding the incremental timing signal.

This observation is inconsistent with previous studies that showed CA1, but not CA3 plays a major role in temporal-order memory for non-spatial information (*31*). This inconsistency may arise from the different time scale used across studies (*32*). For example, a recent rodent lesion study showed that CA3 does play a role in temporal-order memory for odor information when the time interval between the items are small (3-10 s) (*33*). Farovic, Dupont and Eichenbaum suggested that both CA3 and CA1 are engaged in temporal-order memory for items, but they may play different roles. Further studies will be needed to test the latter hypothesis.

In other MTL areas, the item cells tended to distribute in a cluster at anterior ~20 for PRC (*21*) and at anterior ~22 for ERC. The time cells tended to overlap these item-cell clusters but they distributed more widely compared with the item cells.

Supporting figures

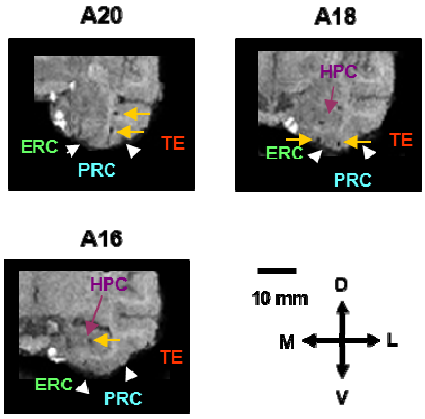

Fig. S1. Ventral parts of three coronal MRI images indicating typical recording sites at 20 mm (A20), 18 mm (A18) and 16 mm (A16) anterior to the interaural line. D, dorsal; V, ventral; M, medial; L, lateral. White arrow heads, borders between ERC and PRC, and between PRC and TE. Yellow arrows indicate metal deposits.

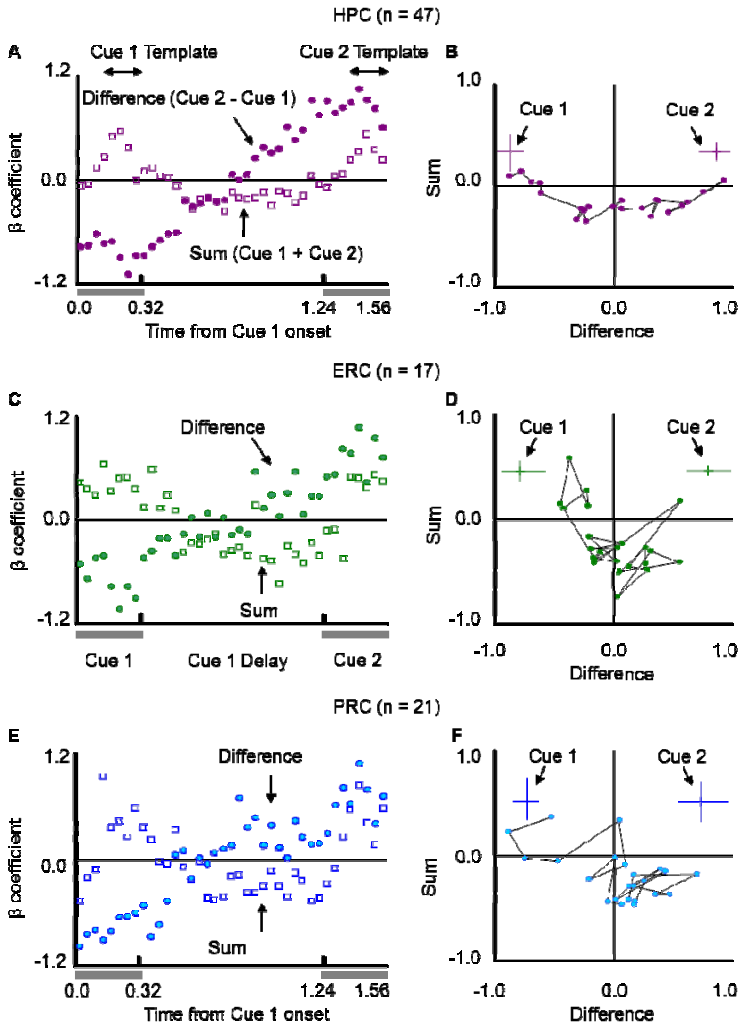

Fig. S2. Temporal dynamics of population vectors projected onto two-dimensional space. (**A**, **C** and **E**) Time courses of β coefficients for the predictors of Cue 2 minus Cue 1 ('difference' shown in filled circles) and Cue 1 plus Cue 2 ('sum' shown in open squares) for HPC, ERC and PRC plotted in 40 ms time bins. Gray rectangles indicate cue presentations. (**B**, **D** and **F**) Scatter plots of the β coefficients for 'difference' and 'sum' during the cue 1 delay period. Consecutive time points were connected by lines. The cue 1 and cue 2 states are represented by crosses indicating means and standard errors. The standard errors were estimated by bootstrap methods (n = 100).

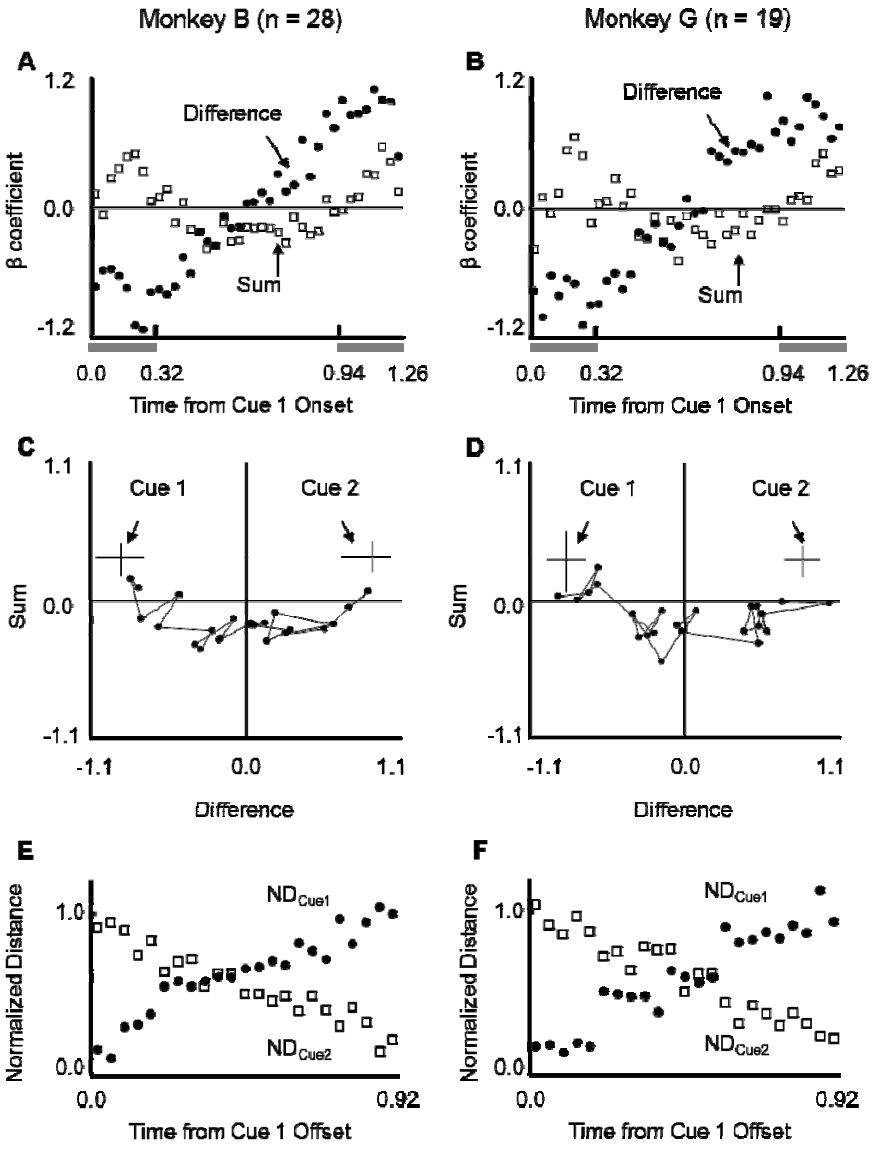

Fig. S3. Temporal dynamics of population vectors in the two animals. Left column shows the results for the HPC time cells from monkey B. Right column shows the results from monkey G. (**A** and **B**) Time courses of β coefficients. The format is the same as that of fig S2 A, C and E. (**C** and **D**) Scatter plots of the β coefficients. The format is the same as that of fig S2 B, D and F. (**E** and **F**) Normalized distances (ND) from the cue 1 states (filled circles) and the cue 2 states (open squares). The format is the same as that of Fig 2 C to E.

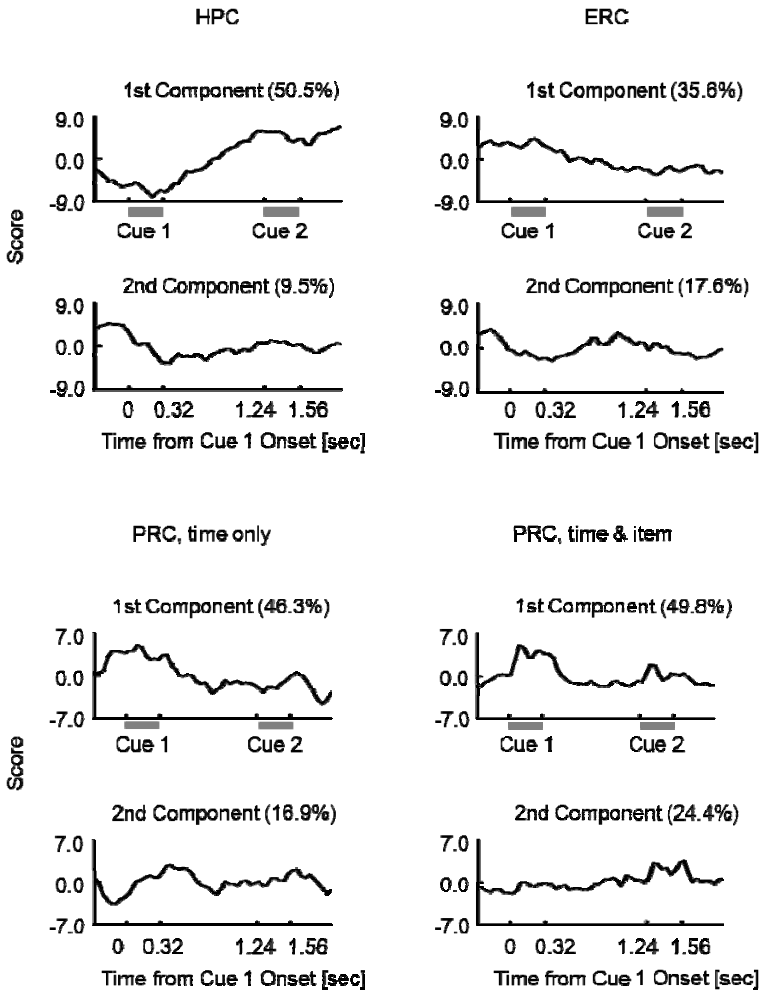

Fig. S4. Principal component analysis of the response properties of time cells in the MTL. The scores of the first (upper) and second (lower) components were plotted against the time during the encoding phase. The principal component analysis was conducted using all the time cells in HPC (n = 47) and ERC (n = 17). For PRC, the time cells were separated into two subgroups: time only cells (n = 14) and time & item cells (n = 7). The numbers in parentheses indicate the proportion of the neural response explained by each principle component. Gray rectangles indicate cue presentations.

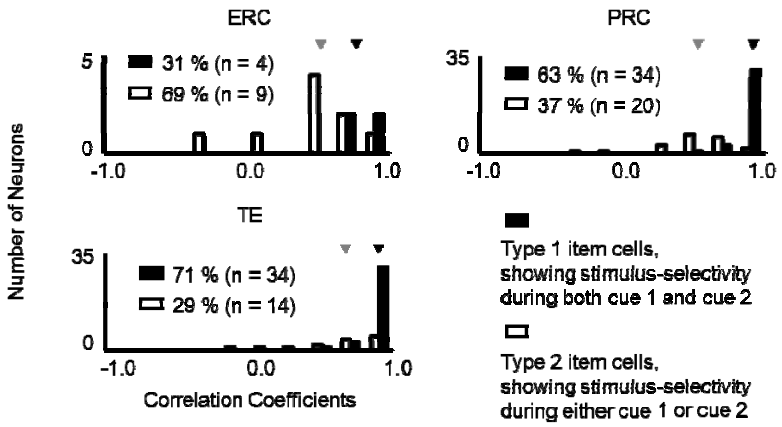

Fig. S5. Distributions of correlation coefficients between cue 1 and cue 2 in ERC, PRC and TE. Ordinates indicate the frequency of neurons in each bin. Black arrow heads, median values for the Type 1 item cells showing stimulus-selectivity during both two cue periods (filled bars). Gray arrow heads, median values for the Type 2 item cells showing stimulus-selectivity during only one of the two cue periods (open bars). The correlation coefficients for the entire populations of item cells in ERC, PRC and TE were significantly different between the two types of item cells ($P < 0.0001$, Kolmogorov-Simonov test), while the correlation coefficients did not differ among the areas for either type of the item cells ($P = 0.12$ for the Type 1 and $P = 0.17$ for the Type 2, Kruskal-Wallis test).

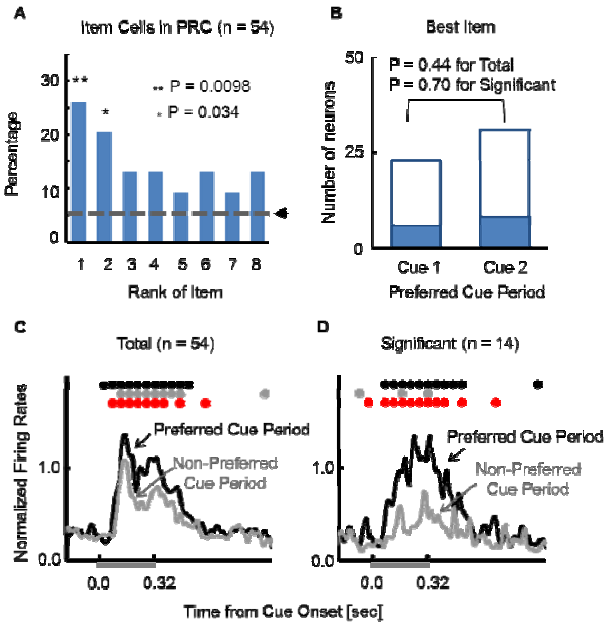

Fig. S6. (**A**) Percentage of the item cells showing significant difference between cue 1 and cue 2 to each rank of item. Dashed line and arrow indicate a chance level (5%). Double asterisks, significantly higher frequency above the chance level (P = 0.0098, chi-square test). Asterisk, P = 0.034. (**B**) Numbers of cue 1 preferring item cells to the best items (item as 1st rank for each neuron) were compared with those of cue 2 preferring item cells. Filled portions indicate the item cells showing significant difference between cue 1 and cue 2. (**C**) Population–averaged (n = 54) normalized responses to the best items. Black lines, responses during the preferred cue period (i.e., cue 1 or cue 2). Gray lines, responses during the non-preferred cue period. The responses were normalized by mean amplitudes during the preferred cue period (80 – 400 ms after cue onset) for individual neurons. Black circles, time bins (40 ms) in which the responses in the preferred cue period were significantly different from those during 300 ms before cue 1 onset (P < 0.05, two-tailed t-test). Gray circles, time bins in which the responses in the non-preferred cue period were significantly different from those during 300 ms before cue 1 onset. Red circles, time bins in which the responses to the preferred cue period were significantly different from those to the non-preferred cue period. (**D**) the same format as (C), but for the time cells showing significant difference between cue 1 and cue 2 (n = 14).

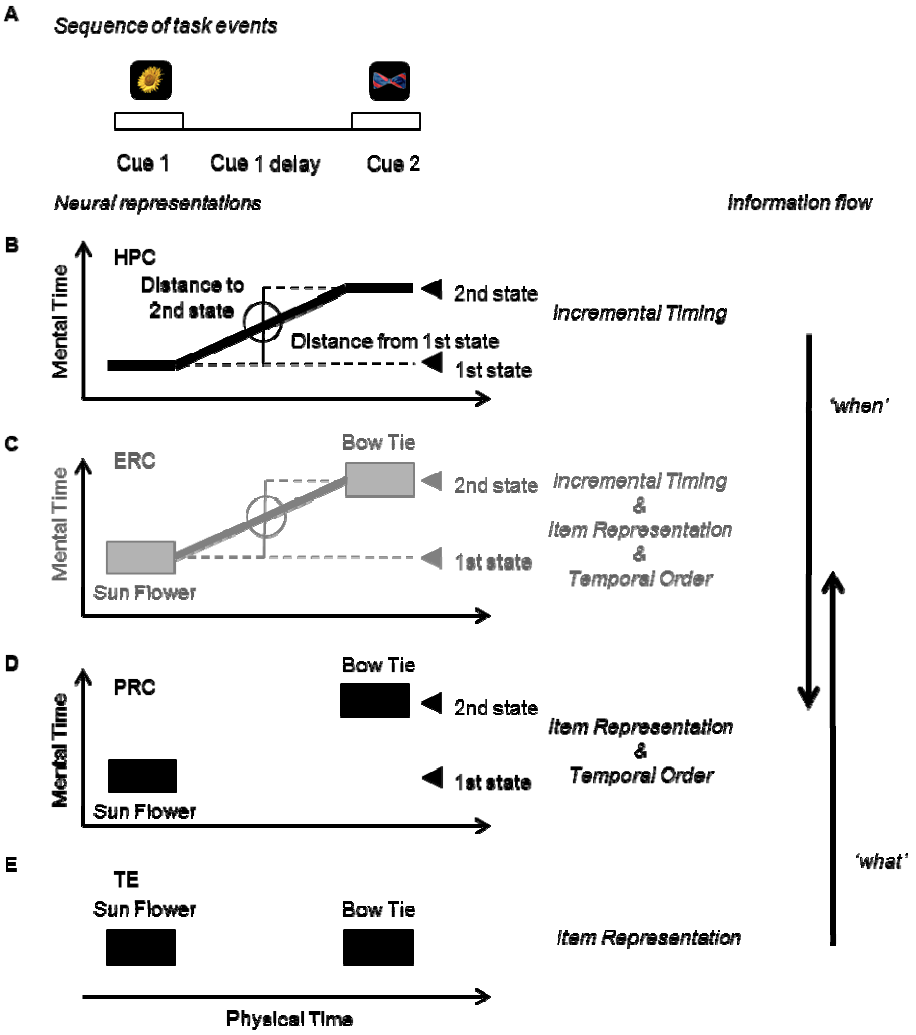

Fig. S7. Complementary representations of temporal-order memory and hypothesized information flow across MTL regions and area TE. (**A**) Schematic diagrams during the encoding phase of the temporal-order memory task where "Sun Flower" was shown as cue 1 and "Bow Tie" was shown as cue 2. (**B** to **E**) Graphs show "mental time" as a function of "physical time" during the encoding phase. Thick angled lines across the cue 1 delay period (B and C) show neuronal states (mental time) at particular time 't' defined by the distances from neuronal states during the 1st and the 2nd item presentations. Filled rectangles in c-e indicate item representations. Weaker overall signals in ERC are shown in gray (B). Two opposite vertical arrows in the right show hypothesized information flows which indicate 'what' (upward) and 'when' (downward), respectively.

Supporting tables

Table S1. Number of neurons showing item and time effects during the encoding phase at a significance level of $P < 0.01$.

	HPC	ERC	PRC	TE
Total				
Recorded	193	143	231	77
Item or Time	53	29	68	50
Item	6	13	54	48
Time	47	17	21	3
Monkey B				
Recorded	112	98	166	63
Item or Time	30	20	39	40
Item	2	9	27	39
Time	28	12	15	1
Monkey G				
Recorded	81	45	65	14
Item or Time	23	9	29	10
Item	4	4	27	9
Time	19	5	6	2

Table S2. Number of neurons in the right and left hemispheres showing item and time effects during the encoding phase at a significance level of $P < 0.01$.

	HPC	ERC	PRC	TE
Right				
Recorded	142	106	187	62
Item or Time	41	21	51	40
Item	3	11	41	39
Time	38	11	14	1
Left				
Recorded	51	37	44	15
Item or Time	12	8	17	10
Item	3	2	13	9
Time	9	6	7	2

Proportions of the task-related neurons (i.e. item or time cells) out of the recorded neurons did not significantly differ between the right and left hemispheres in all the areas ($P > 0.28$ for each area, chi-square test).

Table S3. Mean and standard error of LFP activity in gamma band and beta band during cue 1 and cue 2 periods.

	HPC 62 sites	ERC 54 sites	PRC 49 sites	TE 29 sites
High-Frequency Gamma (70-90 Hz)				
Cue 1	-0.006±0.004] ‡	0.001±0.006	0.036±0.006***	0.087±0.012***
Cue 2	0.040±0.006***	-0.022±0.013	0.042±0.009***	0.086±0.020**
Low-Frequency Gamma (35-50 Hz)				
Cue 1	0.010±0.004*] ‡	0.017±0.005**	0.036±0.005***] †	0.057±0.009***
Cue 2	0.048±0.005***	0.019±0.008*	0.053±0.008***	0.066±0.013**
Beta (15-25 Hz)				
Cue 1	0.040±0.007***	0.030±0.006***	0.078±0.013***	0.110±0.023**
Cue 2	0.031±0.010*	0.047±0.009***	0.070±0.011***	0.098±0.017**

***, $P < 0.0001$; **, $P < 0.001$; *, $P < 0.05$, significantly different activities from the baseline by two-tailed paired t-test.
‡, $P < 0.0001$; †, $P < 0.05$, significantly different activities between cue1 and cue 2 by two-tailed paired t-test

Table S4. Norm of the residuals for 0th, 1st and 2nd order of polynomial curve fittings to the normalized distances from cue 1and cue 2, and their sum during cue 1 delay period.

	HPC	ERC	PRC
Distance from Cue1			
0th order	1.30] ‡	1.06] †	1.49] †
1st order	0.28	0.49	0.89
2nd order	0.25	0.43	0.46] †
Distance from Cue 2			
0th order	1.11] ‡	0.61	0.75
1st order	0.23	0.58	0.62
2nd order	0.23	0.67	0.49
Sum			
0th order	0.28	0.89] †	1.07
1st order	0.21	0.62	0.73
2nd order	0.21	0.73	0.63

‡, $P < 0.0001$; †, $P < 0.05$, significantly differen: variances by f-test

Table S5. Number of neurons showing time and item effects during in HPC subdivisions the encoding phase at a significance level of $P < 0.01$.

	Anterior	Intermediate	Posterior	Total
Dorsal				
Recorded	25	28	33	86
Time	10	9	5	24
Item	0	0	0	0
Ventral				
Recorded	25	35	47	107
Time	3	7	13	23
Item	3	1	2	6
Total				
Recorded	50	63	80	193
Time	13	16	18	47
Item	3	1	2	6

No significant difference in proportions of the time cells out of the recorded neurons across the six subdivisions (P = 0.40, chi-square test).

References and Notes

1. H. Eichenbaum, N. Fortin, Episodic memory and the hippocampus: It's about time. *Curr. Dir. Psychol. Sci.* **12**, 53 (2003). doi:10.1111/1467-8721.01225

2. E. Tulving, Episodic memory: From mind to brain. *Annu. Rev. Psychol.* **53**, 1 (2002). doi:10.1146/annurev.psych.53.100901.135114 Medline

3. J. J. Downes, A. R. Mayes, C. MacDonald, N. M. Hunkin, Temporal order memory in patients with Korsakoff's syndrome and medial temporal amnesia. *Neuropsychologia* **40**, 853 (2002). doi:10.1016/S0028-3932(01)00172-5 Medline

4. F. Vargha-Khadem *et al.*, Differential effects of early hippocampal pathology on episodic and semantic memory. *Science* **277**, 376 (1997). doi:10.1126/science.277.5324.376 Medline

5. M. Moscovitch, L. Nadel, G. Winocur, A. Gilboa, R. S. Rosenbaum, The cognitive neuroscience of remote episodic, semantic and spatial memory. *Curr. Opin. Neurobiol.* **16**, 179 (2006). doi:10.1016/j.conb.2006.03.013 Medline

6. M. W. Howard, M. J. Kahana, A distributed representation of temporal context. *J. Math. Psychol.* **46**, 269 (2002). doi:10.1006/jmps.2001.1388

7. M. W. Howard, M. S. Fotedar, A. V. Datey, M. E. Hasselmo, The temporal context model in spatial navigation and relational learning: Toward a common explanation of medial temporal lobe function across domains. *Psychol. Rev.* **112**, 75 (2005). doi:10.1037/0033-295X.112.1.75 Medline

8. L. J. Jenkins, C. Ranganath, Prefrontal and medial temporal lobe activity at encoding predicts temporal context memory. *J. Neurosci.* **30**, 15558 (2010). doi:10.1523/JNEUROSCI.1337-10.2010 Medline

9. S. Tubridy, L. Davachi, Medial temporal lobe contributions to episodic sequence encoding. *Cereb. Cortex* **21**, 272 (2011). doi:10.1093/cercor/bhq092 Medline

10. E. Pastalkova, V. Itskov, A. Amarasingham, G. Buzsáki, Internally generated cell assembly sequences in the rat hippocampus. *Science* **321**, 1322 (2008). doi:10.1126/science.1159775 Medline

11. P. R. Gill, S. J. Mizumori, D. M. Smith, Hippocampal episode fields develop with learning. *Hippocampus* n/a (2010). doi:10.1002/hipo.20832 Medline

12. J. R. Manns, M. W. Howard, H. Eichenbaum, Gradual changes in hippocampal activity support remembering the order of events. *Neuron* **56**, 530 (2007). doi:10.1016/j.neuron.2007.08.017 Medline

13. W. A. Suzuki, D. G. Amaral, Perirhinal and parahippocampal cortices of the macaque monkey: Cortical afferents. *J. Comp. Neurol.* **350**, 497 (1994). doi:10.1002/cne.903500402 Medline

14. Y. Naya, M. Yoshida, Y. Miyashita, Backward spreading of memory-retrieval signal in the primate temporal cortex. *Science* **291**, 661 (2001). doi:10.1126/science.291.5504.661 Medline

15. S. Wirth *et al*., Single neurons in the monkey hippocampus and learning of new associations. *Science* **300**, 1578 (2003). doi:10.1126/science.1084324 Medline

16. K. Tanaka, Inferotemporal cortex and object vision. *Annu. Rev. Neurosci.* **19**, 109 (1996). doi:10.1146/annurev.ne.19.030196.000545 Medline

17. Y. Ninokura, H. Mushiake, J. Tanji, Representation of the temporal order of visual objects in the primate lateral prefrontal cortex. *J. Neurophysiol.* **89**, 2868 (2003). doi:10.1152/jn.00647.2002 Medline

18. M. R. Warden, E. K. Miller, The representation of multiple objects in prefrontal neuronal delay activity. *Cereb. Cortex* **17** (suppl. 1), i41 (2007). doi:10.1093/cercor/bhm070 Medline

19. Information on materials and methods are available on *Science* Online.

20. O. Barak, M. Tsodyks, R. Romo, Neuronal population coding of parametric working memory. *J. Neurosci.* **30**, 9424 (2010). Medline

21. Y. Naya, M. Yoshida, Y. Miyashita, Forward processing of long-term associative memory in monkey inferotemporal cortex. *J. Neurosci.* **23**, 2861 (2003). Medline

22. S. R. Lehky, T. J. Sejnowski, R. Desimone, Selectivity and sparseness in the responses of striate complex cells. *Vision Res.* **45**, 57 (2005). doi:10.1016/j.visres.2004.07.021 Medline

23. R. Paz *et al.*, A neural substrate in the human hippocampus for linking successive events. *Proc. Natl. Acad. Sci. U.S.A.* **107**, 6046 (2010). doi:10.1073/pnas.0910834107 Medline

24. K. W. Koyano et al., In vivo visualization of single-unit recording sites using MRI-detectable elgiloy deposit marking. *J. Neurophysiol.* **105**, 1380 (2011). doi:10.1152/jn.00358.2010 Medline

25. R. Fujimichi *et al*., Unitized representation of paired objects in area 35 of the macaque perirhinal cortex. *Eur. J. Neurosci.* **32**, 659 (2010). doi:10.1111/j.1460-9568.2010.07320.x Medline

26. J. K. Jun *et al*., Heterogenous population coding of a short-term memory and decision task. *J. Neurosci.* **30**, 916 (2010). doi:10.1523/JNEUROSCI.2062-09.2010 Medline

27. M. R. Jarvis, P. P. Mitra, Sampling properties of the spectrum and coherency of sequences of action potentials. *Neural Comput.* **13**, 717 (2001). doi:10.1162/089976601300014312 Medline

28. B. Pesaran, J. S. Pezaris, M. Sahani, P. P. Mitra, R. A. Andersen, Temporal structure in neuronal activity during working memory in macaque parietal cortex. *Nat. Neurosci.* **5**, 805 (2002). doi:10.1038/nn890 Medline

29. B. J. Richmond, L. M. Optican, Temporal encoding of two-dimensional patterns by single units in primate inferior temporal cortex. II. Quantification of response waveform. *J. Neurophysiol.* **57**, 147 (1987). Medline

30. M. Yukie, Connections between the medial temporal cortex and the CA1 subfield of the hippocampal formation in the Japanese monkey (*Macaca fuscata*). *J. Comp. Neurol.* **423**, 282 (2000). doi:10.1002/1096-9861(20000724)423:2<282::AID-CNE7>3.0.CO;2-Z Medline

31. E. T. Rolls, R. P. Kesner, A computational theory of hippocampal function, and empirical tests of the theory. *Prog. Neurobiol.* **79**, 1 (2006). doi:10.1016/j.pneurobio.2006.04.005 Medline

32. J. Hoge, R. P. Kesner, Role of CA3 and CA1 subregions of the dorsal hippocampus on temporal processing of objects. *Neurobiol. Learn. Mem.* **88**, 225 (2007). doi:10.1016/j.nlm.2007.04.013 Medline

33. A. Farovik, L. M. Dupont, H. Eichenbaum, Distinct roles for dorsal CA3 and CA1 in memory for sequential nonspatial events. *Learn. Mem.* **17**, 12 (2010). doi:10.1101/lm.1616209 Medline